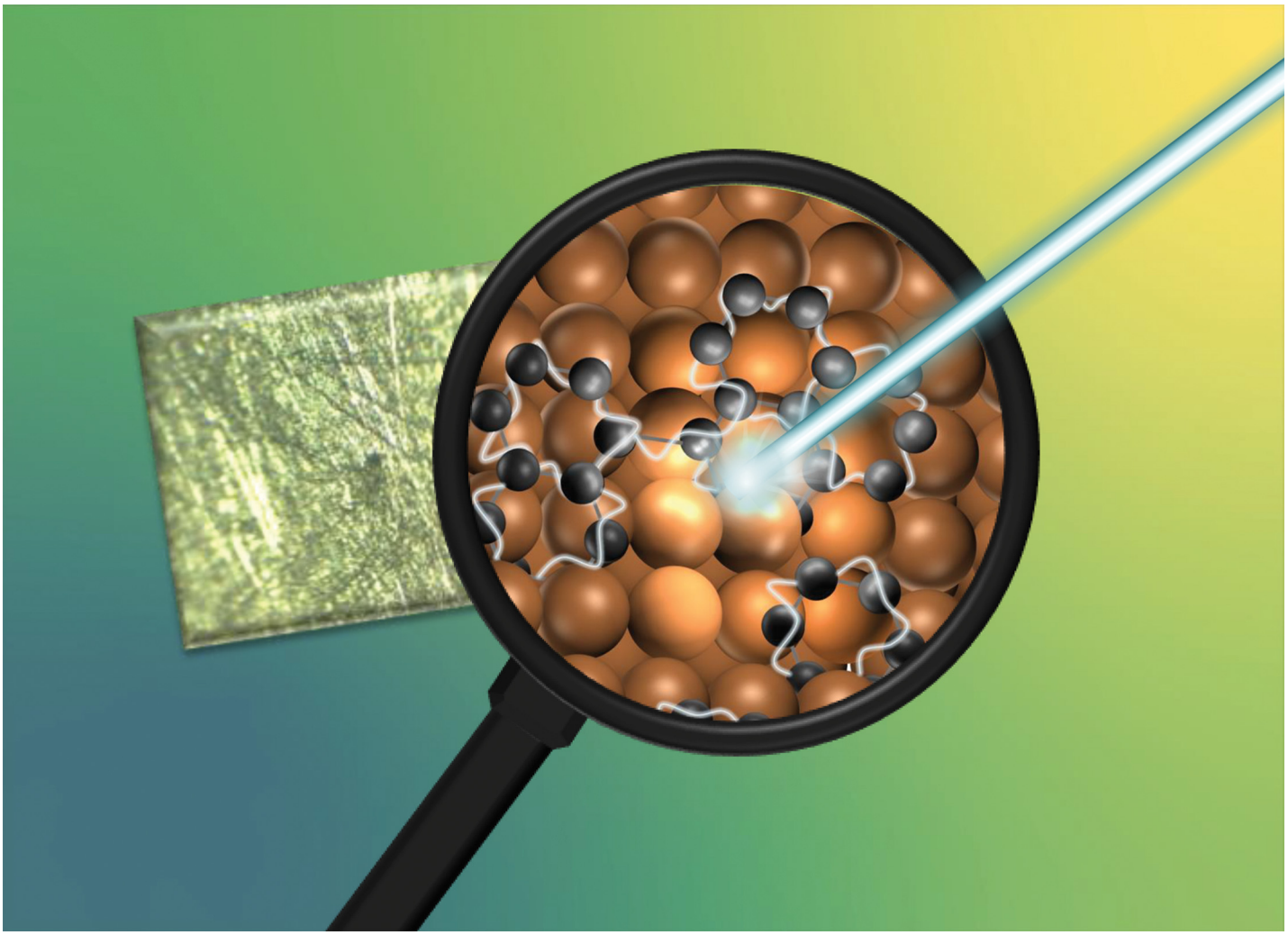

Showcasing research from Professor Emily A. Sprague-Klein's laboratory, Department of Chemistry, Brown University, Providence, Rhode Island USA.

Investigating the mechanism of copper–carbon interactions in ultraconductor materials *via in situ* thermal X-ray and Raman spectroscopy

We investigate novel materials characterized by enhanced thermal conductivity, utilizing advanced thermal X-ray and Raman imaging techniques to elucidate changes in their electronic structure. A notable emergent class of these materials, termed ultraconductors or covetics, is defined by carbon-infused metal structures that exhibit significantly superior electrical and thermal properties relative to their pure metal counterparts. The findings underscore the considerable potential of these materials for a wide range of applications in advanced energy storage technologies.

Cover artwork designed by Elizabeth Donahue.

Image reproduced by permission of Elizabeth Donahue and Emily Sprague-Klein from *Mater. Adv.*, 2025, **6**, 9427.

As featured in:

See E. Sprague-Klein *et al.*, *Mater. Adv.*, 2025, **6**, 9427.

ROYAL SOCIETY OF CHEMISTRY

rsc.li/materials-advances

Registered charity number: 207890

Materials Advances

ROYAL SOCIETY OF CHEMISTRY

PAPER

View Article Online
View Journal | View Issue

Check for updates

Cite this: *Mater. Adv.*, 2025, 6, 9427

Investigating the mechanism of copper–carbon interactions in ultraconductor materials *via in situ* thermal X-ray and Raman spectroscopy

N. Warren,[a] E. Donahue,[a] U. Yunusa,[a] A. Pattammattel,[b] B. Ma[c] and E. Sprague-Klein *[a]

Improving energy transfer efficiency is critical to advancing technologies for a more sustainable future. Nanoscale materials, specifically metal–carbon composites such as ultraconductors, have shown promise in this field due to their enhanced electrical and thermal conductivities. However, the origin of the enhancement has yet to be determined. Prior research has primarily explored these materials at room temperature in an attempt to explain this phenomenon, but these materials have not yet been examined under enhanced thermal conditions. This study probes ultraconductor materials during the heating process to uncover the origins of their enhanced thermal conductivity. Understanding the mechanism underpinning the enhanced properties of the material could lead to increased property enhancement and therefore improved performance in energy transfer technologies. In this work we employ *in situ* thermal X-ray absorption near edge spectroscopy (XANES) and Raman spectroscopy to characterize copper-based covetic materials, revealing how thermal conditions influence the bonding environment and interaction between the copper and infused carbon. Our findings suggest that heating the materials does not result in the formation of chemical bonds between the carbon and copper framework of the material but rather points to a primarily physical interaction within the sample. Furthermore, we hypothesize possible mechanisms underlying the nature of the physical interaction leading to enhanced properties. These insights contribute to a deeper understanding of the material's behavior under relevant thermal conditions and highlight its potential for integration into next-generation energy systems.

Received 16th August 2025,
Accepted 3rd November 2025

DOI: 10.1039/d5ma00916b

rsc.li/materials-advances

Open Access Article. Published on 04 11 2025. Downloaded on 2026/06/02 13:51:55.
This article is licensed under a Creative Commons Attribution-NonCommercial 3.0 Unported Licence.

I. Introduction

Carbon infused metal structures, also known as ultraconductors or covetics, have emerged in the last two decades as promising materials in various sectors due to their enhanced electrical and thermal properties compared to their pure metal counterparts.[1,2] This phenomenon of enhancement has been seen in silver,[3] aluminum,[4,5] copper,[6–8] and other metals.[9] Various techniques have been used to investigate the interacting nature of the infused carbon, such as electron energy loss spectroscopy (EELS), scanning transmission electron microscopy (STEM), X-ray photoelectron spectroscopy (XPS), X-ray diffraction (XRD), and Raman mapping, among others.[2,4,8,10] Many of these studies have shown that the infused carbon exists as nanostructures in sp^2 and sp^3 hybridized states within the metal framework.[2,8–10] Although these carbon nanostructures are believed to play a crucial role in the enhanced conduction properties, the specific understanding of the nature of interactions in these covetic systems under thermal conditions is generally unknown. Such insight into the enhancement mechanism can lead to fabrication of composite materials with improved properties which can ultimately result in their application in electronics and other technologies.

This study focuses on copper based ultraconductors, which have a wide array of potential applications, such as transparent electrodes and efficient electrical wiring.[6,7] Here we show for the first time characterization of the composite structure with *in situ* thermal nano-XANES (X-ray absorption near-edge spectroscopy), and *in situ* thermal Raman spectroscopy. These sensitive techniques are used to better understand the local environment within the material and therefore the nature of the copper–carbon interactions. Our experiments also provide insight to the structure and evolution of the copper ultraconductor species under thermal conditions.

[a] *Department of Chemistry, Brown University, Providence, Rhode Island, USA. E-mail: emily_sprague-klein@brown.edu*
[b] *National Synchrotron Light Source II, Brookhaven National Laboratory, Upton, NY, USA*
[c] *Argonne National Laboratory, Lemont, Illinois, USA*

© 2025 The Author(s). Published by the Royal Society of Chemistry

Open Access Article. Published on 04 11 2025. Downloaded on 2026/06/02 13:51:55.
This article is licensed under a Creative Commons Attribution-NonCommercial 3.0 Unported Licence.

II. Methods

A. Sample generation

Copper materials for X-ray and optical characterization were synthesized according to previously established procedures.[8] Briefly, 0.4% weight carbon infused copper was synthesized *via* electron beam melting using copper powder (99.9% pure metal basis) acquired from Alfa Aesar and carbon powder (>99% purity) acquired from Fisher Chemical.

Precursor powders were prepared by mixing an appropriate amount of copper powder (99.9% pure metal basis, Alfa Aesar, Haverhill, MA) and carbon powder (>99% purity, Fisher Chemical, Waltham, MA) through ball milling. Precautions were taken to minimize copper oxidation by using a nitrogen-filled glovebox for processing, mixing the powders in organic solvent, and drying them in a vacuum oven. The resulting powders were loaded into an e-beam melting hearth with vitreous carbon-coated liner inside an e-beam melting system. A vacuum chamber base pressure of $\sim 1 \times 10^{-7}$ torr was achieved before e-beam melting using an 8.0 kV accelerating voltage and a beam current up to a few hundred milliamps. The position of the electron beam was controlled by a pair of low inductance *x*- and *y*-coils with dynamic defocusing capability. This allows independent motion in the *x*- and *y*-directions, which permits electromagnetic stirring of the molten liquid inside the liner crucible. After melting, samples were rapidly cooled under a vacuum. Because the e-beam hearth was water cooled, the processed material solidified almost instantly after turning off the power to the hearth. After the melted nugget in the hearth reached room temperature, the vacuum chamber was backfilled with nitrogen to ambient pressure, the chamber door was opened, and the produced sample was retrieved. Specimens of appropriate sizes were prepared from the resulting materials for electrical, thermal, microscopy, and spectroscopy characterizations. Details of the operation conditions for making covetic materials by e-beam melting were reported elsewhere.[8,11]

B. Nano-XANES preparation and measurements

Samples with a thickness of ~1 micrometer were cut from bulk material with a FEI Helios 600 NanoLab Focused Ion Beam (FIB) using a gallium source. Samples were platinum welded using a FIB Omniprobe tip onto MEMS Heating Chips produced by Norcada Inc. (Alberta, Canada) and stored under nitrogen atmosphere to prevent oxidation. Samples were transported to the beamline in sealed vacuum containers prior to measurement. Fig. S1 demonstrates FIB sample preparation in the SI section.

Nano-XANES measurements were collected at the National Synchrotron Light Source-II (NSLS-II) at Brookhaven National Laboratory, with the Hard X-Ray Nanoprobe (HXN 3-ID) beamline. Nano-XANES data was collected by acquiring X-ray fluorescence (XRF) maps at several energy points across the copper K-edge absorption spectrum. A detailed description of the experimental methodology is available elsewhere.[12] Prior to data collection, the X-ray energy was calibrated using Cu K-edge absorption from a copper metal foil. A nanofocused beam was generated using a Fresnel zone plate with an outermost zone width of 25 nm. The sample was raster-scanned under the beam, and XRF spectra were collected at each point using a silicon drift detector positioned at 90° to the incident beam. The sample chamber was pumped down to high vacuum (10^{-6} Torr) to prevent oxidation during data collection. At vacuum, the samples were probed at 31 °C, heated incrementally to 155 °C, then to 280 °C and to 400 °C, probing at each temperature, then cooled back to 31 °C and probed again (see Fig. S10). Before XANES measurements, samples were allowed to equilibrate at a set temperature for 300 s before data collection. Spectra were collected at 31 °C after cooling to help determine if any thermal effects were reversible or irreversible.

C. Raman preparation and measurements

Samples used for Raman analysis were machine-cut to fit aluminum oxide heating crucibles. Samples were then hand sanded with 600 grit sandpaper for five minutes, then hand sanded with 1500 grit sandpaper for five minutes, totaling ten minutes of sanding. Sanding was performed so as to remove the top layer of cuprous oxide that is formed after hours of exposure to air.[13] We noticed that the shiny surface finish of the samples polished 1500 grit SiO_2 sandpaper is comparable to the finish produced by polishing using 9-μm diamond paste. Use of SiO_2 sandpaper is to avoid potential contaminations from any carbon containing materials. Ion-polishing of specimens was conducted using a dual-ion beams Gatan precision ion polishing system (PIPS II, Gatan, Pleasanton, California) operated with argon ions. Finally, samples were rinsed with acetonitrile and briefly dried by blowing with nitrogen before being placed in the confocal Raman microscope setup, a diagram of the Raman setup can be found in (Fig. S7).

Raman spectra were collected using a Witec Alpha 300 Confocal Raman Microscope outfitted with fiber-launched continuous wave diode lasers coupled to a beam expander for microscope objective illumination was used to collect Raman spectra. Samples were illuminated with a 532 nm laser source (WITec, Oxford Instruments) with 6 mW laser power measured at the sample using a ThorLabs Compact Power and Energy Meter Console (Part No. PM100D). A back-illuminated 1024 × 127 pixel format thermoelectrically cooled CCD camera (Andor, Oxford Instruments) was used for data collection. A 600 groove per mm grating with a 500 nm blaze was used during data collection.

A constant flow of N_2 gas was positioned to flow over the sample to prevent oxidation on the surface. A schematic of the Raman setup can be seen in Fig. S7. As with the nano-XANES collection, the sample was probed at 31 °C and heated at the same intervals to 400 °C. Here, a room temperature spectrum was also taken because heating was required to reach 31 °C, however in the nano-XANES configuration, no heat was required to reach 31 °C.

III. Results and discussion

A. Nano-XANES

Nano-XANES was selected for spectroscopic characterization of this material because of its ability to probe the elemental and

© 2025 The Author(s). Published by the Royal Society of Chemistry

Open Access Article. Published on 04 11 2025. Downloaded on 2026/06/02 13:51:55.
This article is licensed under a Creative Commons Attribution-NonCommercial 3.0 Unported Licence.

electronic state of a sample.[14] Additionally, *in situ* thermal XANES has been used to investigate material behavior under enhanced thermal conditions.[15,16] The chemical bonding specificity of the technique is invaluable to elucidating the behavior of the species as it relates to the excitation of core electrons within the element. Specifically, K-edge XANES probes transitions from the metal 1s core orbital to unoccupied electronic states which depend both on the oxidation state of the metal center and the local coordination environment.[17,18] Fig. 1(A) Shows the nano-XANES spectra of the sample at 31 °C, 155 °C, 280 °C, 400 °C, and again at 31 °C after the sample was allowed to cool. The edge of a XANES spectrum is highly sensitive to thermal and electronic changes in the sample where spatial mapping allows for correlation between the material's electronic structure and surface morphology for individual sampling points. Importantly, the position of the Cu-K edge of our XANES spectra at 8975 eV is indicative of a properly aligned system as it agrees with previous literature.[19,20]

One challenge of studying and applying copper materials is their rapid oxidation under O_2 rich environments, such as ambient atmosphere. It is imperative to ensure sample integrity and prevent oxidation, so that the spectroscopic features can be related to the internal structure of the composite material. Prior X-ray studies on transition metal oxide and carbide materials (Cu, Co, Fe) have shown energetic shifts in the edge energies or changes in peak intensity due to thermo-catalytic redox transitions in the atomic metal sites because of *in situ* heating.[21–23] Our XANES results, shown in Fig. 1, indicate this is not the case with carbon ultraconductor materials under thermal conditions. We support our findings with spectral information to rule out the presence of copper oxidation during the experiments as a possible explanation for new peaks in the thermal XANES data. Copper–oxygen bonds measured with XANES typically appear at 8985 and 9000 eV.[24–26] The lack of spectral peaks at these energies, shown as dotted vertical lines in Fig. 1(A), provide spectral evidence that the sample has not oxidized. The spectral changes can therefore be attributed to the interaction of the infused carbon nanostructure within the metal sample and localized changes in the electronic structure. Furthermore, the lack of shift in the edge position of the XANES spectra supports the fact that no oxidation occurred in the sample during these experiments.[20]

Fig. 1(A) shows spectral changes as the temperature shifts, as well as a permanent change in the material after the heating process, which is apparent when considering the 31 °C sample before (yellow) and after (dark green) the heating has taken place. As the temperature is sequentially increased from 31 °C to 155 °C and then to 280 °C followed by heating to 400 °C, we observe pronounced peak intensity changes in the rising edge region between 8980 eV and 9000 eV. No changes are observed due to increased temperature in the pre-edge region (8950 eV to 8975 eV) nor at the edge itself (8975 eV) indicating no change in the net oxidation state or coordination geometry of the Cu metal centers. The absence of new peaks in the rising edge due to heating also indicates no appreciable chemical interaction effects between the Cu and C centers due to heating.

Since we have established that no chemical bond formation has taken place, we can further analyze the observed spectral changes to gather insight to the physical interaction of the two components. Overall, the shape of the nano-XANES spectra indicate that the copper sample is in the FCC crystal structure, as seen by the rising edge the feature at ~8982 eV, labelled peak a in Fig. 1(A), as well as the splitting of the white line into two features at ~8993 eV and ~9003 eV.[27,28] As the sample is

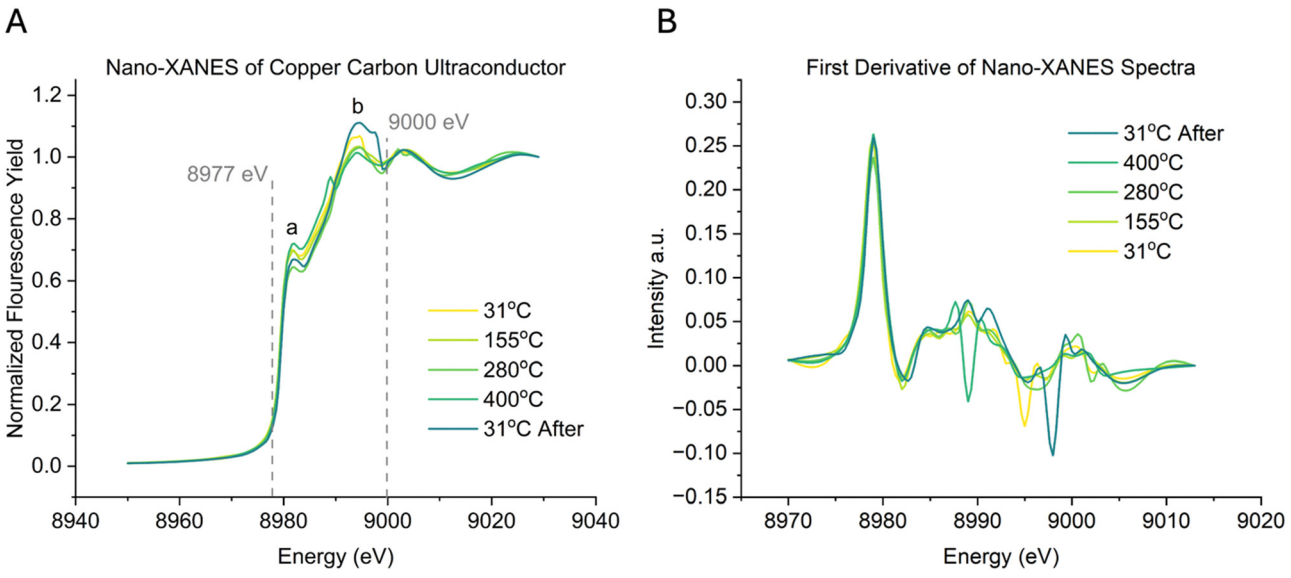

Fig. 1 (A) Cu-K edge nano-XANES spectra of 0.4% wt carbon infused copper at 31 °C, 155 °C, 280 °C, 400 °C, and at 31 °C after heating and cooled back down to room temperature. Dotted lines at 8977 and 9000 eV represent expected locations of copper–oxygen bonds upon formation of copper-oxide layer. Peak a at ~8982 eV is associated with 1s to 4p transition of copper. Peak b at ~8993 eV is associated with scattering events in the outer coordination spheres. (B) The first derivative of the nano-XANES spectra from (A) at varying temperatures.

Open Access Article. Published on 04 11 2025. Downloaded on 2026/06/02 13:51:55.
This article is licensed under a Creative Commons Attribution-NonCommercial 3.0 Unported Licence.

heated, we notice two main changes in the nano-XANES spectra. The first is a change of intensity the edge feature labelled peak a in Fig. 1(A). This peak is associated with the 1s to 4p transition of copper.[19,27] We notice initially that this feature decreases in intensity as the sample is heated from 31 °C to 280 °C, then peaks in intensity at 400 °C and decreases after the sample is cooled to room temperature. This is an observed change reversible with temperature. The second major shift in the sample occurs at ~8993 eV, labelled peak b in Fig. 1(A). This is the first feature of the white line splitting, which as previously mentioned is characteristic of FCC copper. This peak is associated with scattering events in the fourth and fifth coordination spheres.[25,29] This peak intensity decreases as the sample is heated from room temperature to 400 °C. After cooling the intensity increases, indicating an irreversible change in the sample.

Fig. 2 shows post-edge nano-XANES spectra at varying spots on the sample, revealing changes in the local bonding

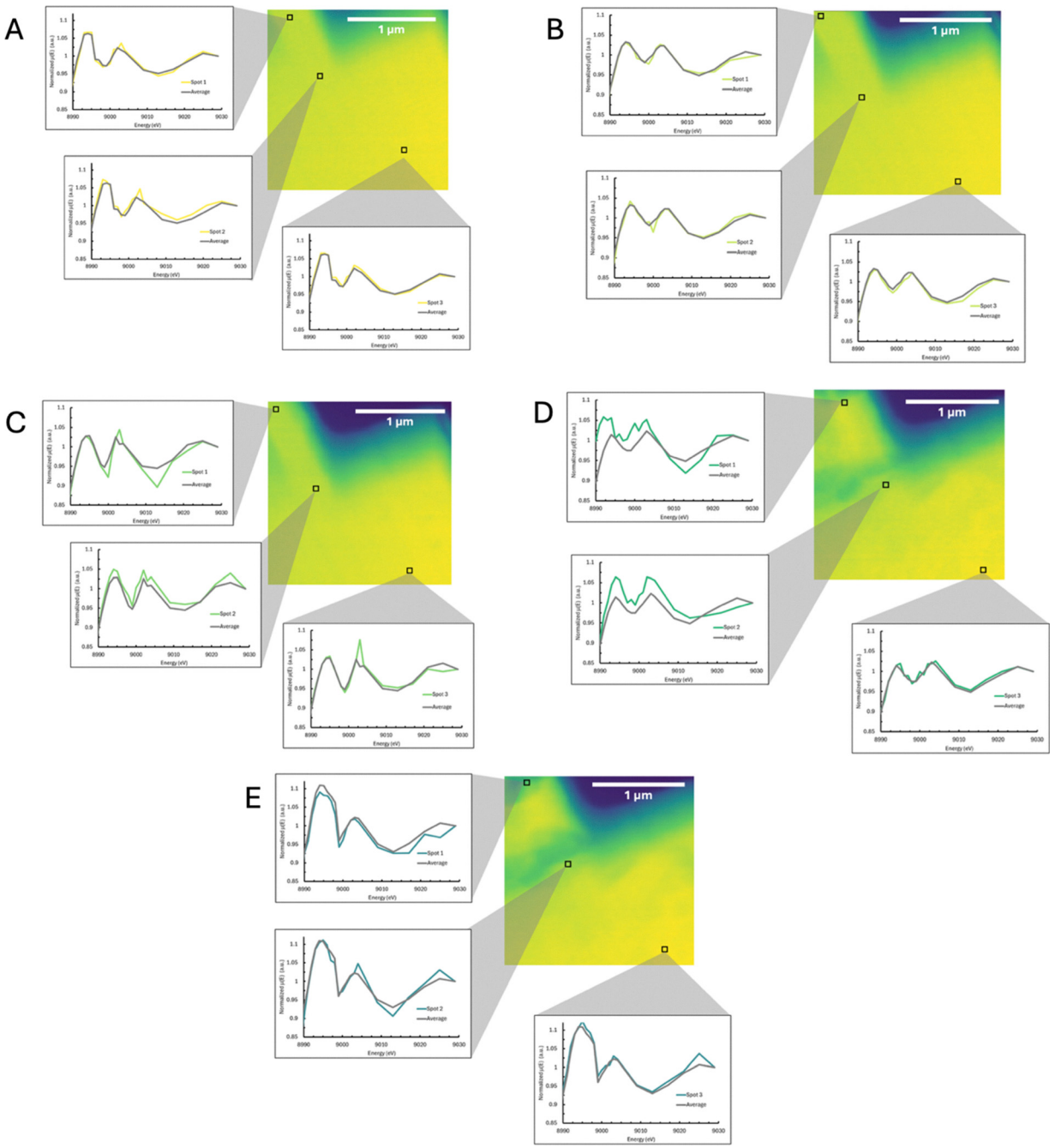

Fig. 2 Post-edge nano-XANES spectra at varying spots at (A) 31 °C, (B) 155 °C, (C) 280 °C, (D) 400 °C, and (E) 31 °C after heating. The average spectrum for each full sample at the respective temperature is shown with a grey line, the colored line represents the spectrum at the indicated point. Significant spectral differences are shown at each temperature. The scale bar in each XANES image represents ~1 μm.

© 2025 The Author(s). Published by the Royal Society of Chemistry

Open Access Article. Published on 04 11 2025. Downloaded on 2026/06/02 13:51:55.
This article is licensed under a Creative Commons Attribution-NonCommercial 3.0 Unported Licence.

environment. Each subfigure represents data taken at a separate temperature point, with the grey line on each plot representing the average spectrum for the entire sample area, and the colored line representing the spectrum at the indicated spot. There are notable differences between the average spectrum at a given temperature and the spectra at an indicated spot. This is caused by the inhomogeneity in carbon distribution within the copper matrix resulting from material synthesis, a well-documented phenomenon with these materials.[2,8,9]

B. Raman spectra

The nature of interactions among components in materials under high temperature conditions can be significantly different from that under ambient conditions, which can ultimately induce changes in bonding and material's structure.[30] Raman spectroscopy can provide information about these changes at different temperatures and can therefore elucidate the nature of copper–carbon interactions within the ultraconductor sample.[31] Additionally, *in situ* thermal Raman spectroscopy has been used to investigate material behavior under enhanced thermal conditions.[32,33]

With the confocal Raman microscope configuration used in this experiment, distinct Raman spectra can be collected for different spots on the sample, such as the two different spots on the covetic material shown in Fig. 3. Spot 1 shows a defect on the surface, in the form of a dark patch surrounded by lighter colored and more lustrous material. Spot 2, however, shows only the metallic material. The confocal Raman microscope configuration enables the correlation of spectral data with each of these visually distinct spots.

The Raman spectra corresponding to each of these spots reveal that they have differing chemical compositions. Fig. 4 shows the Raman spectra of each of these spots at varying temperatures. Individual spectra can be found in (Fig. S2 and S3).

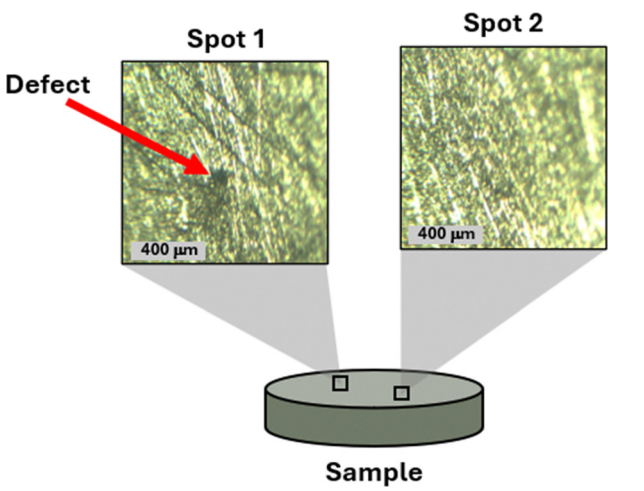

Fig. 3 Schematic of spot 1 and spot 2 found on 0.4% wt carbon sample with corresponding images from confocal Raman spectrometer. Spot 1 shows a significant defect and spot 2 does not, presumably this leads to their varying Raman spectra. The scale bar for each spot represents 400 μm.

Spectra taken at spot 1 show distinct Raman peaks at ~1350 cm^{-1}, 1580 cm^{-1}, and 2700 cm^{-1}, indicated by dotted vertical lines in Fig. 4. Spot 2, however, shows no distinct Raman peaks at any temperature. Similar to the nano-XANES analysis, spectral evidence can be used to indicate a lack of oxidation of the sample during collection. While many distinct copper–oxygen peaks have energies below ~600 cm^{-1}, which is outside the spectral window of this experiment, one Cu–O stretching mode at ~1100 cm^{-1} is visible in the probed window.[34–37] There is no evidence in the collected spectra at either sample spot that the material has oxidized between preparation and data collection, indicative of air-free sample preparation prior to measurements.

The peaks shown on spot 1 can be attributed to the presence of sp^2 hybridized carbon, which confirms the findings of previous studies.[2,8–10] The ~1350 cm^{-1}, ~1580 cm^{-1}, and 2700 cm^{-1} peaks correspond to the D, G, and 2D peaks of sp^2 hybridized carbon, respectfully.[10,38] Sp^2 hybridized carbon can be in the form of graphene, when only few layers are present, or graphite, when thousands of layers of graphene are present. This distinction is important because the various allotropes of carbon each have distinct mechanical, thermal, and electronic properties.[39–44]

The shape and positioning of the D, G, and 2D Raman peaks can provide insight to the graphene or graphite identity of the carbon nanostructures. For example, the positions of the D and 2D peaks can red-shift as laser power increases.[45] In this study, however, the same laser power was used throughout the entirety of the experiment to mitigate this effect. Spectral evidence can be used to corroborate the lack of laser-induced spectral shifting effects as Fig. 4 shows a constant peak position across all temperatures for the features at ~1350 cm^{-1}, 1580 cm^{-1}, and ~2700 cm^{-1}. Fig. S2 shows Raman spectra of spot 2 with no offset, which further confirms that there is no peak shift as the sample temperature changes.

The 2D peak specifically can be related to the number of layers of graphene in the carbon nanostructure.[38] This effect is also dependent on the laser wavelength being used. Considering the findings of Ferrari *et al.*, the shape of the 2D peak centered at roughly 2700 cm^{-1} with ~500 nm laser excitation is consistent with a carbon structure comprised of multiple layers of graphene. Additionally, the ratio of peaks can be considered when determining identification. Ferrari *et al.*, found that with a laser excitation of 514 nm, the 2D peak intensity is much higher than that of the G peak for a graphene sample, whereas the 2D peak is slightly smaller than the G peak for a graphite sample. The spectra in Fig. 4 show a 2D peak of lower intensity than the G peak, further suggesting the presence of multiple layers of graphene, or possibly graphite, in this sample. Furthermore, the defect seen with the confocal Raman microscope at spot 1 is roughly 150 μm in diameter, which is large enough to facilitate multiple layers of graphene assuming the sheets are stacked perpendicular to the sample surface. Considering all these factors, it is likely that the carbon nanostructure found *via* Raman spectroscopy is comprised of at least multiple sheets of graphene.

Open Access Article. Published on 04 11 2025. Downloaded on 2026/06/02 13:51:55.
This article is licensed under a Creative Commons Attribution-NonCommercial 3.0 Unported Licence.

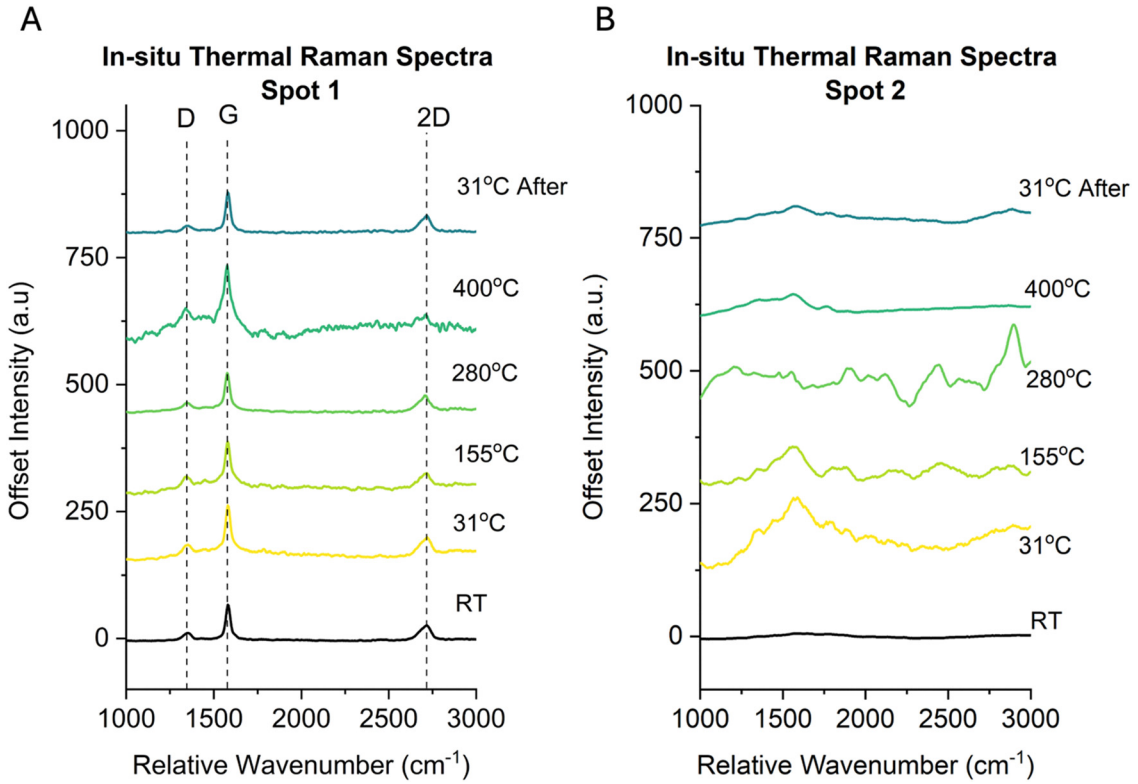

Fig. 4 *In situ* thermal Raman spectra at varying temperature points for spot 1 (A) and for spot 2 (B). The grey vertical lines (left) represent the D (1350 cm^{-1}), G (1580 cm^{-1}), and 2D (2700 cm^{-1}) peaks of sp^2 hybridized carbon. Raman peaks are consistent for spot 1 whereas no clear Raman peaks are present at spot 2 for any temperature.

Overall, across the different temperatures probed, the D, G, and 2D peaks shown at spot 1 remain fairly consistent in shape, position, and intensity. Additional analysis of D, G, and 2D peak intensities and ratios are available in Fig. S5 and S6. The lack of significant change in the Raman spectra across the temperature range suggest the absence of structural phase transition or significant bond formation or breaking upon heating.[46] This supports the evidence of a physical interaction between copper and carbon that plays a key role in the bulk sample properties at varying temperatures, which is a possible explanation for the origin of a thermal enhancement mechanism often observed in metal ultraconductors.

It should be noted that despite the increased noise present in the spectrum taken at 400 °C, the spectrum taken at 31 °C afterwards shows a lack of degradation of the graphite in the sample. This demonstrates stability of this material across a wide range of temperatures, which is promising for practical applications.

C. Discussion

By analyzing the results of nano-XANES and Raman spectroscopy together, we can develop a more comprehensive understanding of the behavior or copper ultraconductors under enhanced thermal conditions. The nano-XANES provides electronic and local structure information of copper, while the Raman spectroscopy probes the hybridization state of the infused carbon. Together these methods offer a new perspective of the ultraconductor materials.

Critically, both measurements provide no evidence of copper-oxide formation on the sample. Spectral changes of nano-XANES and Raman spectroscopy can therefore be attributed to the interaction between the copper lattice and the interstitial carbon. Moreover, both techniques independently point to the same conclusion regarding the nature of copper–carbon interactions within the material. Neither result suggests that there is a chemical bond formation between the copper and infused carbon, leading us to the conclusion that the enhancement mechanism is physical in nature, not chemical.

A recent computational study by Subedi *et al.* investigated electron transport in copper–graphene systems.[47] The results of their study showed that the conductivity of the material increases with a decreasing copper–graphene distance, caused by a copper–graphene–copper bridging within the material. Additionally, the group found that with decreasing interfacial copper–graphene distance, the electronic density of states shows increased contribution from both the copper and graphene atoms, resulting in enhanced conduction properties. This confirms, as our studies suggest, that a physical interaction between copper and carbon can lead to increased conductivity. Thus, we can consider that the heating of the copper ultraconductor in some way leads to a decreased interfacial distance between the lattice and infused carbon. There are

© 2025 The Author(s). Published by the Royal Society of Chemistry

Open Access Article. Published on 04 11 2025. Downloaded on 2026/06/02 13:51:55.
This article is licensed under a Creative Commons Attribution-NonCommercial 3.0 Unported Licence.

numerous mechanisms which could result in this effect, such as copper expansion, an increase interstitial carbon, expansion of the infused graphite, or a combination of each of these.

Overall, we observe no appreciable modification of the local atomic charge and d-band structure of the copper upon heating. Such negligible electronic effect can be expected for systems incorporating atoms with relatively low electronegativity/electron density such as carbon.[48,49] Additionally, the different thermal expansion coefficients between graphene and copper could be causing lattice structure rearrangements.[9,10] These factors provide support for the hypothesis that during heating, the copper could be expanding, or the fraction of carbon which occupy interstitial sites of copper is increased. Both of which lead to a decrease in average copper–carbon interface distance. This change in the copper lattice or interstitial site occupation by atomistic carbon within the copper matrix could explain the changes seen in the XANES spectrum over the varying temperatures. As previously mentioned, there is no change in oxidation state of the copper, *i.e.* no bond forms between copper and carbon during heating. Thus, the accumulation of carbon in the lattice voids of the copper matrix during heating induces the disruption of the local lattice which could be the primary driver of the enhanced conduction properties.[50–54]

Expansion of the graphite could also potentially lead to a decreased interfacial distance within the sample, however experimental conditions and spectral evidence can be used to rule out this mechanism. Expanded graphite can be produced by heating, resulting in increased gaps between the graphene layers.[55] A recent study by Coetzee *et al.* reported that spectral changes can indicate the level of layer expansion within the graphite.[56] Specifically, the ratio between G and D peak intensity will change significantly upon expansion. Considering the experimental method used in our study as well as the resulting spectra, we can determine that this is likely not occurring in our sample. Critically, a rapid increase in temperature is required for graphite expansion to occur. The treatment of graphite and rapid temperature increase to $\sim$900 °C or more results in a gas explosion, causing the layers of graphene to expand.[57] Our sample is heated slowly over time, and only to 400 °C. In other words, our experimental setup is not likely to cause the expansion of graphene layers. Additionally, our results show no statistically significant change in the G peak : D peak ratio (seen in Fig. S6) which we would expect to see based on the study by Coetzee *et al.* Considering these two factors, we can speculate that graphite expansion is likely not occurring in our sample.

IV. Conclusion

Using the complementary techniques of *in situ* thermal nano-XANES and Raman spectroscopy, we observe that the underlying nature of the copper–carbon interaction within copper ultraconductors is physical, not chemical. Nano-XANES measurements show no edge shift or peak formation indicating that copper does not oxidize and/or form a formal bond to carbon during heating. Additionally, *in situ* Raman spectra reveal that the infused sp^2 carbon does not experience bond formation or breaking during heating. This is reflected in the consistent Raman peak intensity, position, and shape of graphitic carbon. These techniques independently suggest the same conclusion, leading us to speculate that the enhanced conduction of the bulk material is the result of a physical interaction between copper and infused carbon.

We propose that the increased conductivity may be caused by a reduction in interfacial distance between copper and graphene, which is known to result in enhanced conduction. A few processes could lead to this decrease in distance, such as copper expansion, an increase interstitial carbon, or expansion of the infused graphite. However, graphite expansion is unlikely due to experimental conditions and stable Raman spectra.

Further studies, including time-resolved experiments, are required to confirm our proposed mechanism of reduced interfacial copper–graphene distance as the cause of increased conduction in copper ultraconductors. Additionally, other factors such as carbon loading, structural reconstructions and pressure may also influence the interaction between the copper lattice and infused carbon. A deeper understanding of these interactions under thermal conditions is essential to explain bulk material properties and further optimize ultraconductor materials as they are integrated into advanced technologies, such as powering the national grid, that involve conducting heat and electricity more efficiently than conventional metals.

Conflicts of interest

The authors have no conflict of interest to disclose.

Data availability

The data supporting this article have been included as part of the supplementary information (SI). Supplementary information is available. See DOI: **https://doi.org/10.1039/d5ma00916b**.

Acknowledgements

This work was supported by Brown University startup funds and National Science Foundation Award 2429239. This research used resources HXN-3-ID of the National Synchrotron Light Source II, a U.S. Department of Energy (DOE) Office of Science User Facility operated for the DOE Office of Science by Brookhaven National Laboratory under contract no. DE-SC0012704. Data shown here was collected using resources from Instrumentation for Molecular and Nanoscale Innovation (IMNI) NanoTools Facility and Electron Microscopy Facility. Work at Argonne National Laboratory was supported by the U.S. Department of Energy, Office of Electricity, under contract no. DE-AC02-06CH11357. The authors acknowledge D. Schauer for insightful discussion.

Open Access Article. Published on 04 11 2025. Downloaded on 2026/06/02 13:51:55.
This article is licensed under a Creative Commons Attribution-NonCommercial 3.0 Unported Licence.

References

1 Y. Wang, X. Zhang, X. Ding, Y. Li, P. Zhang, M. Shu, Q. Zhang, Y. Gong, K. Zheng, B. Wu and X. Tian, Enhanced thermal conductivity of carbon nitride-doped graphene/polyimide composite film *via* a 'deciduous-like' strategy, *Compos. Sci. Technol.*, 2021, **205**, 108693.
2 M. Bakir and I. Jasiuk, Novel metal-carbon nanomaterials: A review on covetics, *Adv. Mater. Lett.*, 2017, **8**(9), 884–890.
3 L. G. Salamanca-Riba, R. A. Isaacs, M. C. LeMieux, J. Wan, K. Gaskell, Y. Jiang, M. Wuttig, A. N. Mansour, S. N. Rashkeev, M. M. Kuklja, P. Y. Zavalij, J. R. Santiago and L. Hu, Synthetic Crystals of Silver with Carbon: 3D Epitaxy of Carbon Nanostructures in the Silver Lattice, *Adv. Funct. Mater.*, 2015, **25**(30), 4768–4777.
4 H. M. I. Jaim, R. A. Isaacs, S. N. Rashkeev, M. Kuklja, D. P. Cole, M. C. LeMieux, I. Jasiuk, S. Nilufar and L. G. Salamanca-Riba, Sp2 carbon embedded in Al-6061 and Al-7075 alloys in the form of crystalline graphene nanoribbons, *Carbon*, 2016, **107**, 56–66.
5 X. Ge, C. Klingshirn, M. Wuttig, K. Gaskell, P. Y. Zavalij, Y. Liang, C. M. Shumeyko, D. P. Cole and L. G. Salamanca-Riba, Mechanism studies and fabrication for the incorporation of carbon into Al alloys by the electro-charging assisted process, *Carbon*, 2019, **149**, 203–212.
6 R. A. Isaacs, H. M. I. Jaim, D. P. Cole, K. Gaskell, O. Rabin and L. G. Salamanca-Riba, Synthesis and characterization of copper-nanocarbon films with enhanced stability, *Carbon*, 2017, **122**, 336–343.
7 R. A. Isaacs, H. Zhu, C. Preston, A. Mansour, M. LeMieux, P. Y. Zavalij, H. M. I. Jaim, O. Rabin, L. Hu and L. G. Salamanca-Riba, Nanocarbon-copper thin film as transparent electrode, *Appl. Phys. Lett.*, 2015, **106**(19), 193108.
8 B. Ma, U. Balachandran, J. Wang, J. Wen, T. H. Lee, S. E. Dorris and A. J. Rondinone, Structural hierarchy of nanocarbon in copper covetics, *Appl. Phys. Lett.*, 2018, **113**(17), 173102.
9 D. Rana, K. Lachmayr and S. R. Lustig, A review of covetics – current understanding and future perspectives, *Nanoscale Adv.*, 2023, **5**(1), 11–26.
10 H. M. I. Jaim, D. P. Cole and L. G. Salamanca-Riba, Characterization of carbon nanostructures in Al and Ag covetic alloys, *Carbon*, 2017, **111**, 309–321.
11 B. Ma, U. Balachandran, S. E. Dorris, T. H. Lee and A. J. Rondinone, Preparation and electrical conductivity of graphitic carbon-infused copper alloys, *MRS Commun.*, 2019, **9**(1), 137–143.
12 A. Pattammattel, R. Tappero, M. Ge, Y. S. Chu, X. Huang, Y. Gao and H. Yan, High-sensitivity nanoscale chemical imaging with hard X-ray nano-XANES, *Sci. Adv.*, 2020, **6**(37), eabb3615.
13 E. Touzé and C. Cougnon, Study of the air-formed oxide layer at the copper surface and its impact on the copper corrosion in an aggressive chloride medium, *Electrochim. Acta*, 2018, **262**, 206–213.
14 A. Pattammattel, R. Tappero, D. Gavrilov, H. Zhang, P. Aronstein, H. J. Forman, P. A. O'Day, H. Yan and Y. S. Chu, Multimodal X-ray nano-spectromicroscopy analysis of chemically heterogeneous systems, *Metallomics*, 2022, **14**(10), mfac078.
15 A. Wadehra, O. Oraby, R. Chahal, A. Levy, H. Yan, Q. Ma, U. Pal, S. Lam and K. Ludwig, Exploring the Local Structure of Molten NaF-ZrF_4 through *In Situ* XANES/EXAFS and Molecular Dynamics, *J. Phys. Chem. B*, 2025, **129**(19), 4747–4755.
16 A. Donatini, P. Georges, T. Fevre, L. Cormier and D. R. Neuville, Charge Transfer Between Ce and Fe During Cooling of an Aluminosilicate Melt: An *In Situ* XANES Investigation, *Inorg. Chem.*, 2025, **64**(7), 3528–3540.
17 M. Bauer and C. Gastl, X-Ray absorption in homogeneous catalysis research: the iron-catalyzed Michael addition reaction by XAS, RIXS and multi-dimensional spectroscopy, *Phys. Chem. Chem. Phys.*, 2010, **12**(21), 5575.
18 E. I. Solomon, R. K. Szilagyi, S. DeBeer George and L. Basumallick, Electronic Structures of Metal Sites in Proteins and Models: Contributions to Function in Blue Copper Proteins, *Chem. Rev.*, 2004, **104**(2), 419–458.
19 R. Zhang and J.-S. McEwen, Local Environment Sensitivity of the Cu K-Edge XANES Features in Cu-SSZ-13: Analysis from First-Principles, *J. Phys. Chem. Lett.*, 2018, **9**(11), 3035–3042.
20 A. Gaur, B. D. Shrivastava and S. K. Joshi, Copper K-edge XANES of Cu(I) and Cu(II) oxide mixtures, *J. Phys.: Conf. Ser.*, 2009, **190**, 012084.
21 S. Boccato, R. Torchio, S. Anzellini, E. Boulard, F. Guyot, T. Irifune, M. Harmand, I. Kantor, F. Miozzi, P. Parisiades, A. D. Rosa, D. Antonangeli and G. Morard, Melting properties by X-ray absorption spectroscopy: common signatures in binary Fe–C, Fe–O, Fe–S and Fe–Si systems, *Sci. Rep.*, 2020, **10**(1), 11663.
22 B. Liu, M. M. Van Schooneveld, Y.-T. Cui, J. Miyawaki, Y. Harada, T. O. Eschemann, K. P. De Jong, M. U. Delgado-Jaime and F. M. F. De Groot, *In Situ* 2p3d Resonant Inelastic X-ray Scattering Tracking Cobalt Nanoparticle Reduction, *J. Phys. Chem. C*, 2017, **121**(32), 17450–17456.
23 J.-J. Velasco-Vélez, C.-H. Chuang, D. Gao, Q. Zhu, D. Ivanov, H. S. Jeon, R. Arrigo, R. V. Mom, E. Stotz, H.-L. Wu, T. E. Jones, B. Roldan Cuenya, A. Knop-Gericke and R. Schlögl, On the Activity/Selectivity and Phase Stability of Thermally Grown Copper Oxides during the Electrocatalytic Reduction of CO_2, *ACS Catal.*, 2020, **10**(19), 11510–11518.
24 T. Lais, L. Lukashuk, L. Van De Water, T. I. Hyde, M. Aramini and G. Sankar, Elucidation of copper environment in a Cu–Cr–Fe oxide catalyst through *in situ* high-resolution XANES investigation, *Phys. Chem. Chem. Phys.*, 2021, **23**(10), 5888–5896.
25 Y. Liu, N. Marcella, J. Timoshenko, A. Halder, B. Yang, L. Kolipaka, M. J. Pellin, S. Seifert, S. Vajda, P. Liu and A. I. Frenkel, Mapping XANES spectra on structural descriptors of copper oxide clusters using supervised machine learning, *J. Chem. Phys.*, 2019, **151**(16), 164201.
26 M. A. Artsiusheuski, O. Safonova, D. Palagin, J. A. Van Bokhoven and V. L. Sushkevich, Structural Evolution of

© 2025 The Author(s). Published by the Royal Society of Chemistry

Open Access Article. Published on 04 11 2025. Downloaded on 2026/06/02 13:51:55.
This article is licensed under a Creative Commons Attribution-NonCommercial 3.0 Unported Licence.

Copper-Oxo Sites in Zeolites upon the Reaction with Methane Investigated by Means of Cu K-edge X-ray Absorption Spectroscopy, *J. Phys. Chem. C*, 2023, **127**(20), 9603–9615.

27 A. A. Guda, S. A. Guda, A. Martini, A. N. Kravtsova, A. Algasov, A. Bugaev, S. P. Kubrin, L. V. Guda, P. Šot, J. A. Van Bokhoven, C. Copéret and A. V. Soldatov, Understanding X-ray absorption spectra by means of descriptors and machine learning algorithms, *npj Comput. Mater.*, 2021, **7**(1), 203.

28 J. L. Alfke, A. Müller, A. H. Clark, A. Cervellino, M. Plodinec, A. Comas-Vives, C. Copéret and O. V. Safonova, BCC-Cu nanoparticles: from a transient to a stable allotrope by tuning size and reaction conditions, *Phys. Chem. Chem. Phys.*, 2022, **24**(39), 24429–24438.

29 G. Greaves, P. Durham, G. Diakun and P. Quinn, Near-edge X-ray absorption spectra for metallic Co and Mn, *Nature*, 1981, **294**(2), 139–142.

30 C.-S. Yoo, Chemistry under extreme conditions: Pressure evolution of chemical bonding and structure in dense solids, *Matter Radiat. Extremes*, 2020, **5**(1), 018202.

31 K. I. Hadjiivanov, D. A. Panayotov, M. Y. Mihaylov, E. Z. Ivanova, K. K. Chakarova, S. M. Andonova and N. L. Drenchev, Power of Infrared and Raman Spectroscopies to Characterize Metal–Organic Frameworks and Investigate Their Interaction with Guest Molecules, *Chem. Rev.*, 2021, **121**(3), 1286–1424.

32 M. Sheng, J. You, X. Xia, G. Liu, Y. Zhao, F. Xu, L. Zhang, Q. Zhang, S. Wan, L. Lu and K. Tang, *In Situ* High-Temperature Raman Spectroscopy and Simulations for Correlating Structure Evolution with Viscosity in the Binary Potassium Titanate System, *Anal. Chem.*, 2025, **97**(23), 12379–12388.

33 D. Bondar, A. Canizarès, D. Bilardello, P. Valdivia, A. Zandonà, C. Romano, M. Allix and D. Di Genova, Nanolite Crystallization in Volcanic Glasses: Insights From High-Temperature Raman Spectroscopy and Low-Temperature Rock-Magnetic Analysis, *Geochem., Geophys., Geosyst.*, 2025, **26**(1), e2024GC011846.

34 S. Choudhary, J. V. N. Sarma, S. Pande, S. Ababou-Girard, P. Turban, B. Lepine and S. Gangopadhyay, Oxidation mechanism of thin Cu films: A gateway towards the formation of single oxide phase, *AIP Adv.*, 2018, **8**(5), 055114.

35 M. Rashad, M. Rüsing, G. Berth, K. Lischka and A. Pawlis, CuO and Co_3O_4 Nanoparticles: Synthesis, Characterizations, and Raman Spectroscopy, *J. Nanomater.*, 2013, **2013**(1), 714853.

36 K. A. Jagadish and D. Kekuda, Thermal annealing effect on phase evolution, physical properties of DC sputtered copper oxide thin films and transport behavior of ITO/CuO/Al Schottky diodes, *Appl. Phys. A: Mater. Sci. Process.*, 2024, **130**(5), 315.

37 S. Dolai, R. Dey, S. Das, S. Hussain, R. Bhar and A. K. Pal, Cupric oxide (CuO) thin films prepared by reactive d.c. magnetron sputtering technique for photovoltaic application, *J. Alloys Compd.*, 2017, **724**, 456–464.

38 A. C. Ferrari, Raman spectroscopy of graphene and graphite: Disorder, electron–phonon coupling, doping and nonadiabatic effects, *Solid State Commun.*, 2007, **143**(1–2), 47–57.

39 M. F. L. De Volder, S. H. Tawfick, R. H. Baughman and A. J. Hart, Carbon Nanotubes: Present and Future Commercial Applications, *Science*, 2013, **339**(6119), 535–539.

40 K. S. Novoselov, A. K. Geim, S. V. Morozov, D. Jiang, Y. Zhang, S. V. Dubonos, I. V. Grigorieva and A. A. Firsov, Electric Field Effect in Atomically Thin Carbon Films, *Science*, 2004, **306**(5696), 666–669.

41 C. Lee, X. Wei, J. W. Kysar and J. Hone, Measurement of the Elastic Properties and Intrinsic Strength of Monolayer Graphene, *Science*, 2008, **321**(5887), 385–388.

42 A. A. Balandin, S. Ghosh, W. Bao, I. Calizo, D. Teweldebrhan, F. Miao and C. N. Lau, Superior Thermal Conductivity of Single-Layer Graphene, *Nano Lett.*, 2008, **8**(3), 902–907.

43 A. H. Castro Neto, F. Guinea, N. M. R. Peres, K. S. Novoselov and A. K. Geim, The electronic properties of graphene, *Rev. Mod. Phys.*, 2009, **81**(1), 109–162.

44 A. A. Balandin, Thermal properties of graphene and nanostructured carbon materials, *Nat. Mater.*, 2011, **10**(8), 569–581.

45 L. M. Malard, M. A. Pimenta, G. Dresselhaus and M. S. Dresselhaus, Raman spectroscopy in graphene, *Phys. Rep.*, 2009, **473**(5–6), 51–87.

46 A. N. C. Ferreira, W. C. Ferreira, A. V. Duarte, C. C. Santos, P. T. C. Freire, C. Luz-Lima and J. V. B. Moura, *In situ* high-temperature Raman scattering study of monoclinic $Ag_2Mo_2O_7$ microrods, *Spectrochim. Acta, Part A*, 2023, **295**, 122632.

47 K. N. Subedi, K. Nepal, C. Ugwumadu, K. Kappagantula and D. A. Drabold, Electronic transport in copper–graphene composites, *Appl. Phys. Lett.*, 2023, **122**(3), 031903.

48 Y. Nakaya and S. Furukawa, Catalysis of Alloys: Classification, Principles, and Design for a Variety of Materials and Reactions, *Chem. Rev.*, 2023, **123**(9), 5859–5947.

49 S. Scheiner, Carbon as an electron donor atom, *Polyhedron*, 2021, **193**, 114905.

50 Z. Su, T. Shi, J. Yang, H. Shen, Z. Li, S. Wang, G. Ran and C. Lu, The effect of interstitial carbon atoms on defect evolution in high entropy alloys under helium irradiation, *Acta Mater.*, 2022, **233**, 117955.

51 Y. Nakaya, E. Hayashida, R. Shi, K. Shimizu and S. Furukawa, Interstitial Carbon Dopant in Palladium–Gold Alloy Boosting the Catalytic Performance in Vinyl Acetate Monomer Synthesis, *J. Am. Chem. Soc.*, 2023, **145**(5), 2985–2998.

52 S. D. Pike, E. R. White, A. Regoutz, N. Sammy, D. J. Payne, C. K. Williams and M. S. P. Shaffer, Reversible Redox Cycling of Well-Defined, Ultrasmall Cu/Cu_2O Nanoparticles, *ACS Nano*, 2017, **11**(3), 2714–2723.

53 I. A. El-Sesy and Z. M. El-Baradie, Influence carbon and/or iron carbide on the structure and properties of dual-phase steels, *Mater. Lett.*, 2002, **57**(3), 580–585.

54 Y. Niu, X. Huang, Y. Wang, M. Xu, J. Chen, S. Xu, M.-G. Willinger, W. Zhang, M. Wei and B. Zhang, Manipulating interstitial carbon atoms in the nickel octahedral site for highly efficient hydrogenation of alkyne, *Nat. Commun.*, 2020, **11**(1), 3324.

Open Access Article. Published on 04 11 2025. Downloaded on 2026/06/02 13:51:55.
This article is licensed under a Creative Commons Attribution-NonCommercial 3.0 Unported Licence.

55 D. Zhang, W. Zhang, S. Zhang, X. Ji and L. Li, Synthesis of expanded graphite-based materials for application in lithium-based batteries, *J. Energy Storage*, 2023, **60**, 106678.
56 D. Coetzee, T. Rojviroon, S. Niamlang, J. Militký, J. Wiener, J. Večerník, J. Melicheríková and J. Müllerová, Effects of expanded graphite's structural and elemental characteristics on its oil and heavy metal sorption properties, *Sci. Rep.*, 2024, **14**(1), 13716.
57 P. Murugan, R. D. Nagarajan, B. H. Shetty, M. Govindasamy and A. K. Sundramoorthy, Recent trends in the applications of thermally expanded graphite for energy storage and sensors – a review, *Nanoscale Adv.*, 2021, **3**(22), 6294–6309.

© 2025 The Author(s). Published by the Royal Society of Chemistry